nature materials

ARTICLES

PUBLISHED ONLINE: 23 MARCH 2014 | DOI: 10.1038/NMAT3912

Synthesis and patterning of tunable multiscale materials with engineered cells

Allen Y. Chen[1,2,3,4,5], Zhengtao Deng[2,3,4], Amanda N. Billings[3], Urartu O. S. Seker[2,3,4], Michelle Y. Lu[2,3,4], Robert J. Citorik[2,3,4,6], Bijan Zakeri[2,3,4] and Timothy K. Lu[1,2,3,4,6]*

Many natural biological systems—such as biofilms, shells and skeletal tissues—are able to assemble multifunctional and environmentally responsive multiscale assemblies of living and non-living components. Here, by using inducible genetic circuits and cellular communication circuits to regulate *Escherichia coli* curli amyloid production, we show that *E. coli* cells can organize self-assembling amyloid fibrils across multiple length scales, producing amyloid-based materials that are either externally controllable or undergo autonomous patterning. We also interfaced curli fibrils with inorganic materials, such as gold nanoparticles (AuNPs) and quantum dots (QDs), and used these capabilities to create an environmentally responsive biofilm-based electrical switch, produce gold nanowires and nanorods, co-localize AuNPs with CdTe/CdS QDs to modulate QD fluorescence lifetimes, and nucleate the formation of fluorescent ZnS QDs. This work lays a foundation for synthesizing, patterning, and controlling functional composite materials with engineered cells.

Natural multicellular assemblies such as biofilms, shells, and skeletal tissues have distinctive characteristics that would be useful for materials production and patterning[1–9]. They can detect external signals and respond via remodelling, implement patterning across different length scales, and organize inorganic compounds to create biotic–abiotic composites. In this work, such systems provide inspiration for the design of environmentally responsive systems that can integrate biotic and abiotic materials via hierarchical self-assembly. To achieve these capabilities, we engineered artificial gene circuits and self-assembling amyloid fibrils together with synthetic cellular consortia[10–16] and inorganic materials.

Our model system is curli, an extracellular amyloid material produced by *E. coli* that forms fibrils based on the self-assembly of the secreted major curli subunit CsgA (ref. 17). Secreted CsgA monomers are templated on CsgB, which is anchored to the cell surface, to form curli fibrils; moreover, CsgA secreted from one cell can interact with CsgB on other cells[17]. Using synthetic riboregulators[18], we implemented inducible transcriptional and translational control over the expression of CsgA subunits engineered to display various peptide tags, which can interface with inorganic materials. We transformed our synthetic circuits into an *E. coli* MG1655 *PRO* Δ*csgA ompR234* host strain (Supplementary Table 3 and Fig. 20), which has the endogenous *csgA* gene deleted. The *ompR234* mutation enables curli production in liquid media at 30 °C by enhancing the expression of genes from the native curli operon, including *csgB* (refs 19,20). We first introduced histidine-tagged CsgA ($CsgA_{His}$) expression under tight regulation by an anhydrotetracycline (aTc) inducer-responsive riboregulator[18] (Fig. 1a). $CsgA_{His}$ contained two histidine tags, one inserted before the first repeat domain and one inserted after the last repeat domain in CsgA (Supplementary Table 1). The resulting cell strain was designated $aTc_{Receiver}/CsgA_{His}$. Immuno-gold labelling experiments with anti-CsgA antibodies (M. Chapman, University of Michigan[21,22]) showed that curli fibrils were produced only in the presence of aTc (Fig. 1b and Supplementary Fig. 1). Using confocal microscopy, we characterized biofilms formed by $aTc_{Receiver}/CsgA_{His}$ cells augmented with an mCherry-expressing plasmid for convenient visualization. This strain formed biofilms only when induced by aTc, both under static culture conditions (Fig. 1c and Supplementary Fig. 2a) and when cultured in microfluidic flow cells (Fig. 1d and Supplementary Fig. 2b). Biofilm growth was confirmed with a standard crystal-violet (CV) assay (Supplementary Fig. 3). We also quantified curli production with dot blots and found a yield of 63 ± 5.8 (s.e.m.) mg cm^{-3} of biofilm after 24 h (Supplementary Fig. 22).

To create engineered cellular consortia for materials patterning, we built three additional strains: one with CsgA under regulation by an acyl-homoserine lactone (AHL)-inducible riboregulator ($AHL_{Receiver}/CsgA$), one with CsgA under regulation by an aTc-inducible riboregulator ($aTc_{Receiver}/CsgA$), and one with $CsgA_{His}$ under regulation by an AHL-inducible riboregulator ($AHL_{Receiver}/CsgA_{His}$). These strains only produced curli fibrils in the presence of the cognate inducer, demonstrating tight and orthogonal regulation of $csgA_{His}$ expression (Supplementary Fig. 8). Moreover, insertion of heterologous histidine tags did not interfere with curli fibril formation on the basis of Congo Red assays and TEM imaging (Supplementary Figs 4 and 5).

Externally controllable patterning

We engineered consortia composed of $AHL_{Receiver}/CsgA$ and $aTc_{Receiver}/CsgA_{His}$ cells to produce two-component protein fibrils composed of CsgA and $CsgA_{His}$ (Fig. 2). By tuning the pulse lengths and pulse amplitudes of AHL and/or aTc, fibrils with

[1]Biophysics Program, Harvard University, Cambridge, Massachusetts 02138, USA, [2]Department of Electrical Engineering and Computer Science, Massachusetts Institute of Technology, 77 Massachusetts Avenue, Cambridge, Massachusetts 02139, USA, [3]Department of Biological Engineering, Massachusetts Institute of Technology, 77 Massachusetts Avenue, Cambridge, Massachusetts 02139, USA, [4]MIT Synthetic Biology Center, 500 Technology Square, Cambridge, Massachusetts 02139, USA, [5]Harvard-MIT Health Sciences and Technology, Institute for Medical Engineering and Science, 77 Massachusetts Avenue, Cambridge, Massachusetts 02139, USA, [6]MIT Microbiology Program, 77 Massachusetts Avenue, Cambridge, Massachusetts 02139, USA. *e-mail: timlu@mit.edu

© 2014 Macmillan Publishers Limited. All rights reserved.

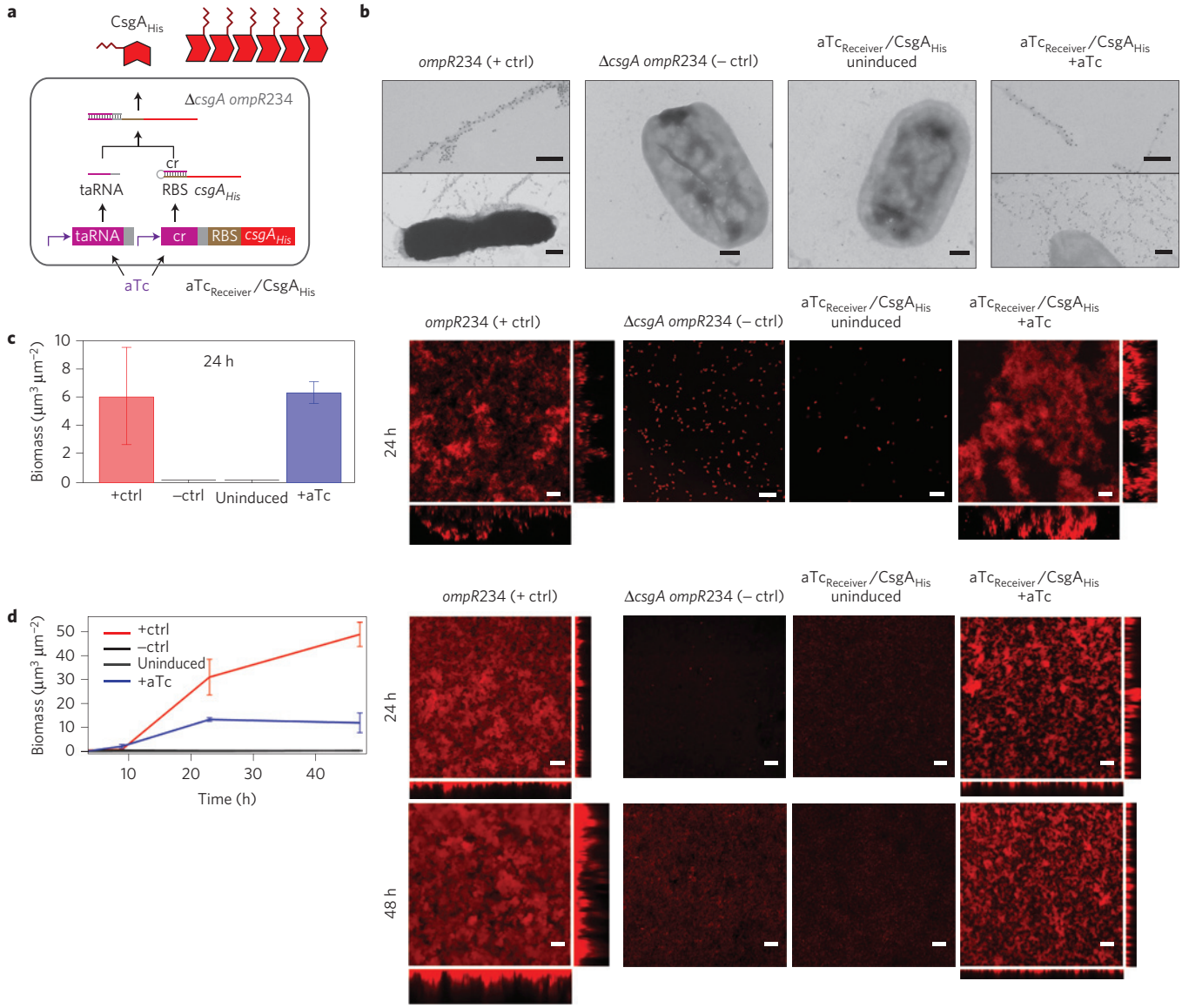

Figure 1 | Inducible production of engineered curli fibrils and biofilms. **a**, Riboregulator circuits tightly regulate expression of curli subunits, such as $CsgA_{His}$. Production of $CsgA_{His}$ requires the expression of *trans*-activating RNA (taRNA). The taRNA prevents the *cis*-repressive (cr) sequence from blocking the ribosome-binding sequence (RBS) controlling translation of the mRNA transcript. In the absence of inducer, mRNA and taRNA levels are low, thus leading to significant repression of gene expression. The addition of aTc induces transcription of both $csgA_{His}$ mRNA and taRNA, thus enabling $CsgA_{His}$ production. Tight regulation of curli expression is useful for controlling patterning (Supplementary Fig. 19). **b**, Immuno-labelling of curli fibrils with rabbit anti-CsgA antibodies and gold-conjugated goat anti-rabbit antibodies. Positive-control ('+ ctrl') MG1655 *ompR234* cells ('*ompR234*', see Supplementary Table 3), which have an intact endogenous *csgA* gene, produce curli fibrils that were labelled by anti-CsgA antibodies and are attached to cells. However, negative-control ('– ctrl') cells with the *csgA* gene knocked out and no *csgA*-expressing circuits ('Δ*csgA ompR234*', see Supplementary Table 3), as well as $aTc_{Receiver}/CsgA_{His}$ cells in the absence of aTc, did not produce curli fibrils. Inducing $aTc_{Receiver}/CsgA_{His}$ cells with aTc enabled the synthesis of curli fibrils that were labelled by anti-CsgA antibodies and attached to cells. Scale bars, 200 nm. **c**, Confocal microscopy and biomass quantification revealed that under static culture conditions, *E. coli ompR234* cells formed thick adherent biofilms. However, *E. coli* Δ*csgA ompR234* cells, as well as $aTc_{Receiver}/CsgA_{His}$ cells in the absence of aTc, did not form biofilms. Inducing $aTc_{Receiver}/CsgA_{His}$ cells with aTc led to the formation of thick adherent biofilms. **d**, Confocal microscopy and biomass quantification revealed similar biofilm-forming capabilities by *E. coli ompR234* and induced $aTc_{Receiver}/CsgA_{His}$ cells when grown in flow cells. To enable visualization, we transformed a constitutive mCherry-expressing plasmid into all strains (Supplementary Methods). Cells were grown in liquid M63 media with glucose; the corresponding experiments for other media conditions are shown in Supplementary Figs 1 and 2. Scale bars in **c**,**d** are 50 μm, and orthogonal XZ and YZ views are maximum-intensity projections.

different structures and compositions were formed. For example, we mixed equal numbers of $AHL_{Receiver}/CsgA$ and $aTc_{Receiver}/CsgA_{His}$ cells together, and induced this mixed-cell population first with AHL, followed by aTc (Fig. 2a). In analogy to block co-polymers, this produced block 'co-fibrils' consisting of blocks of CsgA (unlabelled fibril segments) and blocks of $CsgA_{His}$ (fibril segments labelled by nickel nitrilotriacetic acid-conjugated gold particles 'NiNTA-AuNPs'). NiNTA-AuNPs specifically labelled $CsgA_{His}$-based curli fibrils but not CsgA-based curli fibrils (Supplementary Fig. 9).

© 2014 Macmillan Publishers Limited. All rights reserved.

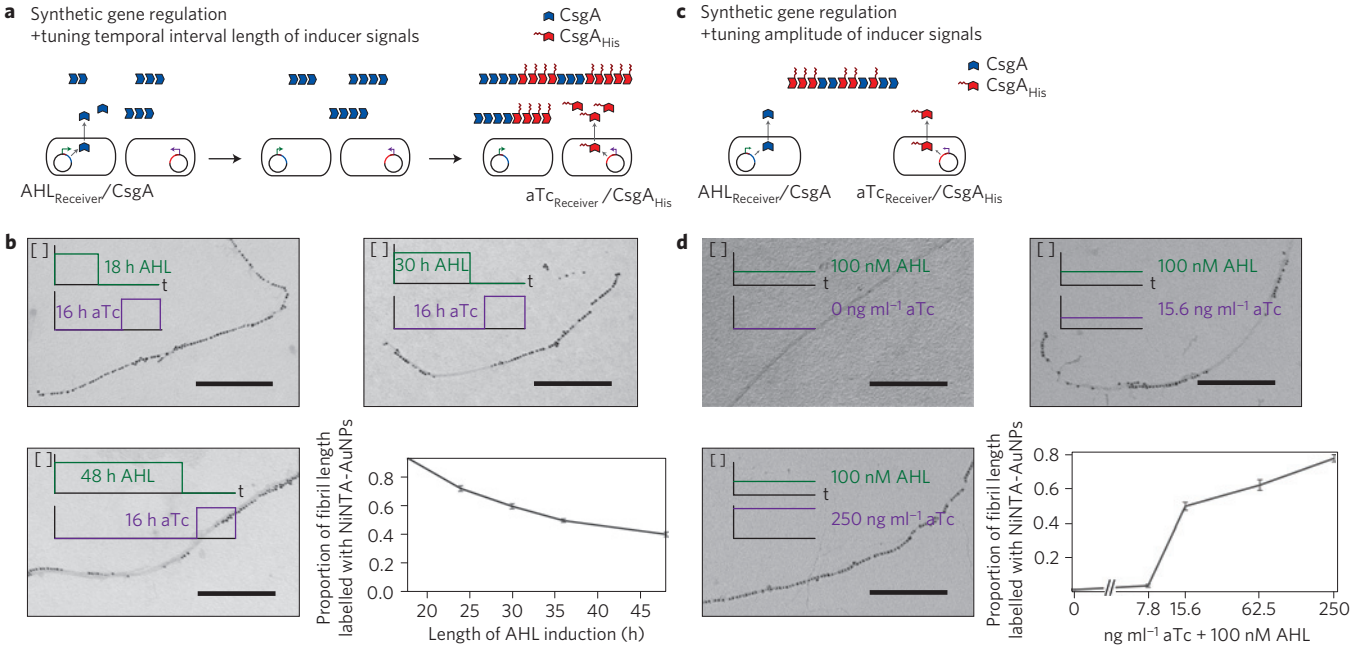

Figure 2 | Conversion of timing and amplitude of chemical inducer signals into material structure and composition. **a**, Inducible synthetic gene circuits couple curli subunit secretion to external chemical inducers. Engineered cells containing these circuits can translate induction pulse length into nanoscale structure and composition of block co-fibrils. **b**, We first used AHL to induce secretion of CsgA from AHL$_{Receiver}$/CsgA, and then used aTc to induce secretion of CsgA$_{His}$ from aTc$_{Receiver}$/CsgA$_{His}$. We tuned the relative block lengths and proportions of CsgA and CsgA$_{His}$ (plot of the proportion of fibril length labelled by NiNTA-AuNP, solid grey line) by changing the relative lengths of AHL versus aTc induction times. Scale bars, 200 nm. **c**, Synthetic genetic regulatory circuits that couple curli subunit secretion to external inducer signals can translate inducer concentration into nanoscale structure and composition of block co-fibrils. **d**, AHL induced secretion of CsgA from AHL$_{Receiver}$/CsgA while, at the same time, aTc induced secretion of CsgA$_{His}$ from aTc$_{Receiver}$/CsgA$_{His}$. We tuned the relative block lengths and proportions of CsgA and CsgA$_{His}$ by changing the relative concentrations of AHL and aTc inducers applied simultaneously. The solid grey line indicates the proportion of fibril length labelled by NiNTA-AuNP with varying concentrations of aTc and constant 100 nM AHL. Detailed histograms can be found in Supplementary Fig. 6. Scale bars, 200 nm.

We tuned the length distribution of the CsgA and CsgA$_{His}$ blocks, as well as the relative proportions of CsgA and CsgA$_{His}$, by changing the relative lengths of AHL pulses versus aTc pulses. As the AHL induction time increased, non-NiNTA-AuNP-labelled fibril segments increased in length, indicating longer CsgA blocks (Fig. 2b and Supplementary Fig. 6a). At the same time, the proportion of fibril length labelled with NiNTA-AuNP decreased, indicating a higher relative proportion of CsgA in the fibrils (Fig. 2b). With temporal separation in expression, the distinct CsgA and CsgA$_{His}$ segments within the block co-fibrils were longer than those in co-fibrils assembled when CsgA and CsgA$_{His}$ were secreted simultaneously with no temporal separation, even though the overall CsgA to CsgA$_{His}$ ratios were similar (Supplementary Fig. 6a). Thus, engineered cells can translate the temporal interval length of input signals into different nanoscale structures and compositions of materials.

We also tuned the length distributions of the two types of blocks, as well as their relative proportions, by inducing simultaneous expression of the CsgA variants with different concentrations of AHL and aTc (Fig. 2c). With AHL-only induction, fibrils were almost uniformly unlabelled; with increasing aTc concentration, the population as well as lengths of unlabelled fibril segments decreased whereas those of labelled fibril segments increased (Fig. 2d and Supplementary Fig. 6b). With aTc-only induction, fibrils were almost uniformly labelled by NiNTA-AuNPs; with increasing AHL concentration, the population as well as lengths of unlabelled segments increased (Supplementary Fig. 7). Thus, engineered cells can translate the amplitudes of input signals, such as inducer concentrations, into different nanoscale structures and compositions of materials.

Autonomous patterning

Cellular communities containing synthetic cellular communication circuits[23–26] can autonomously produce dynamic materials whose structure and composition changes with time (Fig. 3). As *E. coli* does not normally produce AHL, we first engineered an *E. coli* strain that constitutively produces AHL and inducibly produces CsgA in the presence of aTc (AHL$_{Sender}$ + aTc$_{Receiver}$/CsgA). This strain communicated with AHL$_{Receiver}$/CsgA$_{His}$ cells via the diffusible cellular communication signal, AHL. We then combined AHL$_{Sender}$ + aTc$_{Receiver}$/CsgA and AHL$_{Receiver}$/CsgA$_{His}$ cells in varying ratios (Fig. 3a). Induction of this mixed-cell population by aTc resulted in CsgA secretion. Over time, AHL accumulation led to increasing secretion of CsgA$_{His}$, thus generating an increased population and lengths of CsgA$_{His}$ blocks, and a higher relative proportion of CsgA$_{His}$ in material composition (Fig. 3b and Supplementary Fig. 10). The temporal dynamics of changes in material composition was tunable by the initial seeding ratio of AHL$_{Sender}$ + aTc$_{Receiver}$/CsgA to AHL$_{Receiver}$/CsgA$_{His}$ cells (Fig. 3b). When only AHL$_{Sender}$ + aTc$_{Receiver}$/CsgA cells were present, fibrils were almost uniformly unlabelled; when only AHL$_{Receiver}$/CsgA$_{His}$ cells were present, no fibrils were formed (Fig. 3b).

Multiscale patterning

In addition, engineered cellular consortia can achieve spatial control over multiple length scales. Genetic regulation of subunit expression allows fibril patterning from tens of nanometres to micrometres, whereas spatial control at the macroscale can be achieved via spatially varying inducer concentrations. These two methods of control can be combined to create materials patterned across multiple length scales (Fig. 4). To demonstrate this, we

© 2014 Macmillan Publishers Limited. All rights reserved.

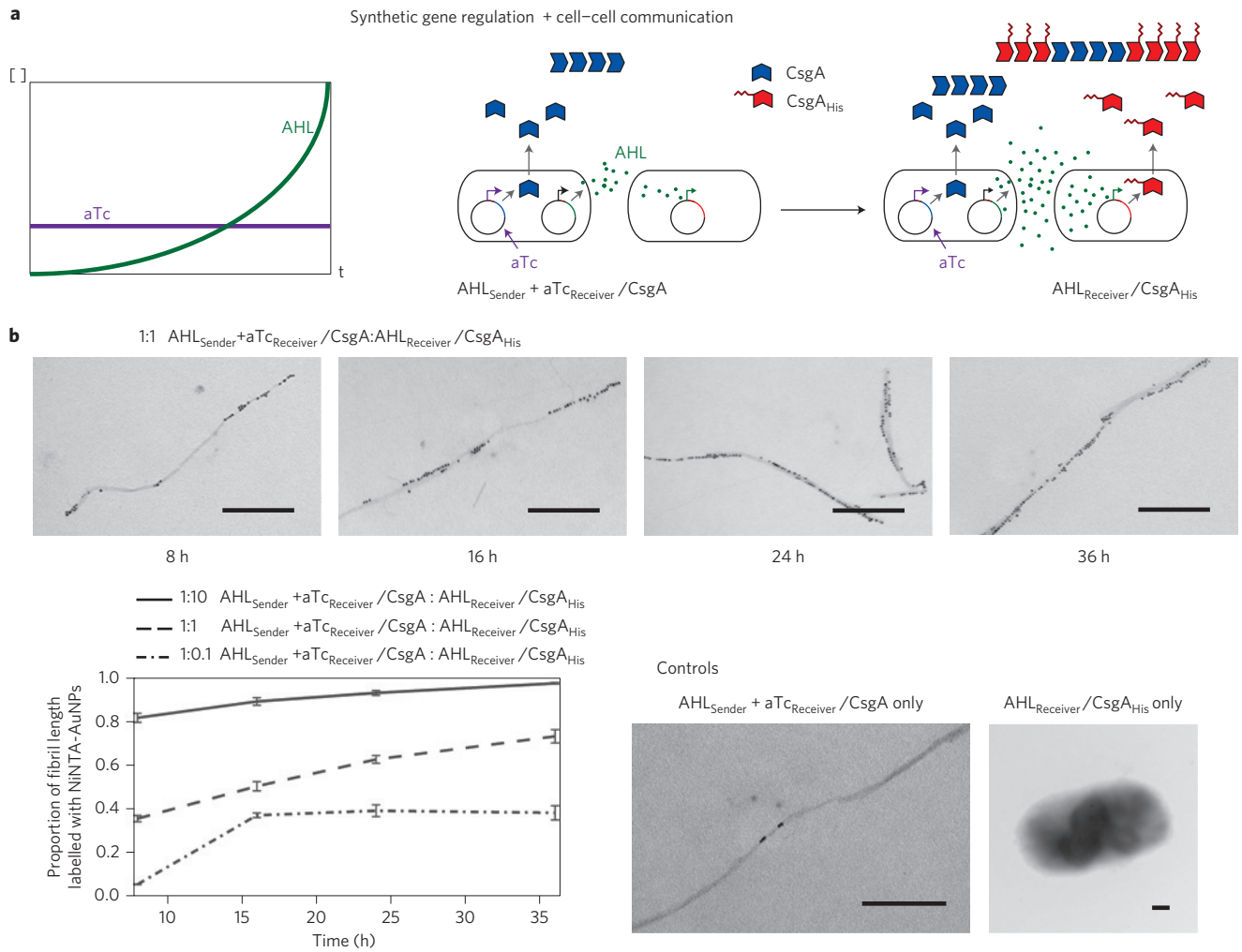

Figure 3 | Synthetic cellular communication for dynamic, autonomous material production and patterning. **a**, Synthetic gene circuits that couple curli subunit secretion to external inducer signals, when combined with synthetic cellular communication circuits, allow for the production of materials whose structure and composition changes autonomously with time. AHL$_{Sender}$+aTc$_{Receiver}$/CsgA secreted both CsgA and AHL. As AHL signal accumulated, AHL$_{Receiver}$/CsgA$_{His}$ secreted increasing levels of CsgA$_{His}$. **b**, Using the autonomous cellular communication system, the length of CsgA$_{His}$ blocks and the proportion of CsgA$_{His}$ increased with time (plot of the proportion of fibril length labelled by NiNTA-AuNP, grey lines). This behaviour could be tuned by the ratio of the seeding density of AHL$_{Sender}$+aTc$_{Receiver}$/CsgA cells to AHL$_{Receiver}$/CsgA$_{His}$ cells. When only AHL$_{Sender}$+aTc$_{Receiver}$/CsgA cells were present, the resulting fibrils were almost uniformly unlabelled; when only AHL$_{Receiver}$/CsgA$_{His}$ cells were present, no curli fibrils were formed (Controls). Detailed histograms can be found in Supplementary Fig. 10. Scale bars, 200 nm.

created agar plates with opposing concentration gradients of AHL and aTc, and overlaid bacterial populations consisting of equal numbers of four cell strains: AHL$_{Receiver}$/CsgA, aTc$_{Receiver}$/CsgA$_{His}$, AHL$_{Receiver}$/GFP, and aTc$_{Receiver}$/mCherry. The AHL$_{Receiver}$/GFP and aTc$_{Receiver}$/mCherry cells enabled visualization of inducer concentration gradients (Fig. 4b and Supplementary Fig. 12). AHL$_{Receiver}$/CsgA and aTc$_{Reciever}$/CsgA$_{His}$ cells secreted different levels of CsgA and CsgA$_{His}$, depending on their positions on the concentration gradient, to generate a spatial gradient of changing fibril structures (Fig. 4a). This multiscale material was patterned at the nanoscale as block co-fibrils, and at the millimetre scale with position-dependent fibril structure (Fig. 4b and Supplementary Fig. 11a). Agar plates without inducer concentration gradients did not generate fibril structures that varied along the plate (Supplementary Fig. 11a).

Protein engineering can also control the structure of cell-produced biomaterials at the nanoscale. We hypothesized that fusing tandem repeats of CsgA together would increase the distance between equivalent positions on adjacent monomers where functional domains can be displayed. Concatenating eight tandem repeats of CsgA and adding a histidine tag to the C-terminus (8XCsgA$_{His}$) resulted in fibrils that were labelled by a syncopated pattern of NiNTA-AuNP, with clusters of particles separated by 33.3 ± 27.1 (s.e.m.) nm (Fig. 4c and Supplementary Fig. 11b). Using this finding, we demonstrated a second example of multiscale assembly. Specifically, we combined equal numbers of AHL$_{Receiver}$/8XCsgA$_{His}$ and aTc$_{Receiver}$/CsgA$_{His}$ cells. We induced this mixed-cell population sequentially with AHL followed by aTc (Fig. 4d) to generate block co-fibrils consisting of 8XCsgA$_{His}$ segments and CsgA$_{His}$ segments patterned across nanometre-to-micrometre scales (Fig. 4d and Supplementary Fig. 11c).

Interfaces with inorganic materials

Our living cell system can be used to create functional materials, such as environmentally switchable conductive biofilms. We hypothesized that aTc-inducible production of CsgA$_{His}$ monomers by aTc$_{Receiver}$/CsgA$_{His}$ cells would generate extracellular amyloid fibrils that organize NiNTA-AuNPs into chains, and form a

© 2014 Macmillan Publishers Limited. All rights reserved.

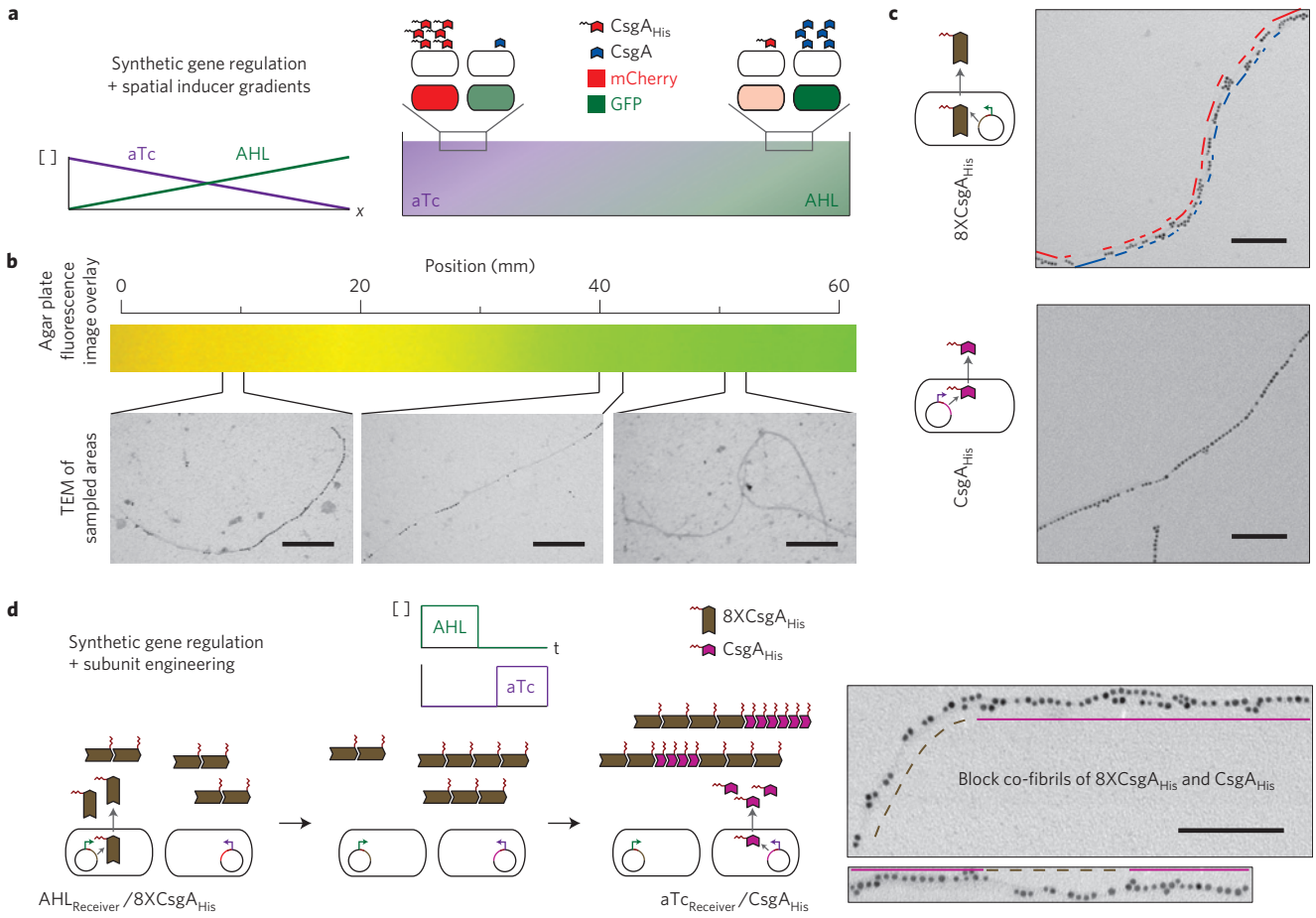

Figure 4 | Multiscale patterning with cellular consortia via synthetic gene regulation combined with inducer gradients and subunit engineering. **a**, Synthetic gene circuits that couple curli subunit secretion to external inducer signals, when combined with a spatial inducer gradient, enable patterning across multiple length scales. We used an agar plate with opposing concentration gradients of AHL and aTc to achieve control at the macroscale (Supplementary Fig. 12). This was combined with regulation of nanoscale patterning to achieve multiscale patterning. Embedded in top agar were equal numbers of AHL$_{Receiver}$/CsgA, aTc$_{Receiver}$/CsgA$_{His}$, AHL$_{Receiver}$/GFP, and aTc$_{Receiver}$/mCherry cells. **b**, By combining synthetic gene regulation with spatial inducer gradients, we created a change in the nanoscale structure of fibrils across a distance of millimetres. This nanoscale and macroscale patterning was shown by changes in segment lengths of unlabelled and NiNTA-AuNP-labelled fibril segments at different locations across the agar plate. Inducer concentration gradients were demonstrated by overlaid GFP and mCherry fluorescence images of embedded AHL$_{Receiver}$/GFP and aTc$_{Receiver}$/mCherry reporter cells. Scale bars, 200 nm. **c**, We also achieved patterning at the nanoscale by protein engineering of curli subunits. Concatenating eight tandem repeats of CsgA and adding one histidine tag to the C-terminus (8XCsgA$_{His}$) resulted in fibrils that were labelled by a syncopated pattern of NiNTA-AuNPs, with clusters of particles separated by 33.3 ± 27.1 (s.e.m.) nm. Scale bars, 100 nm. **d**, Synthetic gene circuits that couple curli subunit secretion to external inducer signals, when combined with subunit engineering, enable patterning across multiple length scales (nanometres to micrometres). We used AHL to induce production of 8XCsgA$_{His}$ from AHL$_{Receiver}$/8XCsgA$_{His}$, and then used aTc to induce production of CsgA$_{His}$ from aTc$_{Receiver}$/CsgA$_{His}$. In the TEM images, dashed brown lines refer to syncopated 8XCsgA$_{His}$ segments while the solid amethyst lines indicate CsgA$_{His}$ segments. Detailed histograms for data shown here can be found in Supplementary Fig. 11. Scale bars, 100 nm.

conductive biofilm network. As shown in Fig. 1, the expression of extracellular curli fibrils enables surface adherence by multicellular bacterial communities, resulting in biofilm formation. Engineered biofilms were grown on interdigitated electrodes deposited on Thermanox coverslips, with aTc$_{Receiver}$/CsgA$_{His}$ cells cultured in the presence of NiNTA-AuNPs and in the presence or absence of aTc inducer (Fig. 5a). We showed by confocal microscopy that biofilms were formed in an aTc-dependent manner (Supplementary Fig. 14). Scanning electron microscopy (SEM), scanning electron microscopy/energy dispersive X-ray spectroscopy (SEM/EDS), and transmission electron microscopy (TEM) were performed to further characterize biofilm samples (Fig. 5b). In the presence of aTc, biofilms formed, spanned electrodes (as shown by SEM imaging), and contained networks of gold that connected electrodes (as shown by SEM/EDS elemental mapping). In contrast, SEM imaging of cells grown in the absence of induction showed only scattered bacteria in the gaps between electrodes, and SEM/EDS showed no gold networks. TEM imaging revealed that aTc-induced biofilms organized gold particles into dense networks (Fig. 5b and Supplementary Fig. 16), whereas samples with cells in the absence of aTc showed only scattered, isolated gold particles (Fig. 5b). Biofilms formed in the presence of aTc had 0.82 ± 0.17 (s.e.m.) nanosiemens conductance, whereas samples with cells in the absence of aTc had no measureable conductance (Supplementary Fig. 15). Biofilms formed with aTc$_{Receiver}$/CsgA$_{His}$ cells induced by aTc, but grown in the absence of NiNTA-AuNPs, had electrical conductance that was two orders of magnitude lower than those formed in the presence of NiNTA-AuNPs (Supplementary Fig. 17a). Samples containing AHL$_{Receiver}$/CsgA$_{His}$ cells grown in the presence of NiNTA-AuNPs and aTc had no measureable conductance (Supplementary Fig. 17b).

© 2014 Macmillan Publishers Limited. All rights reserved.

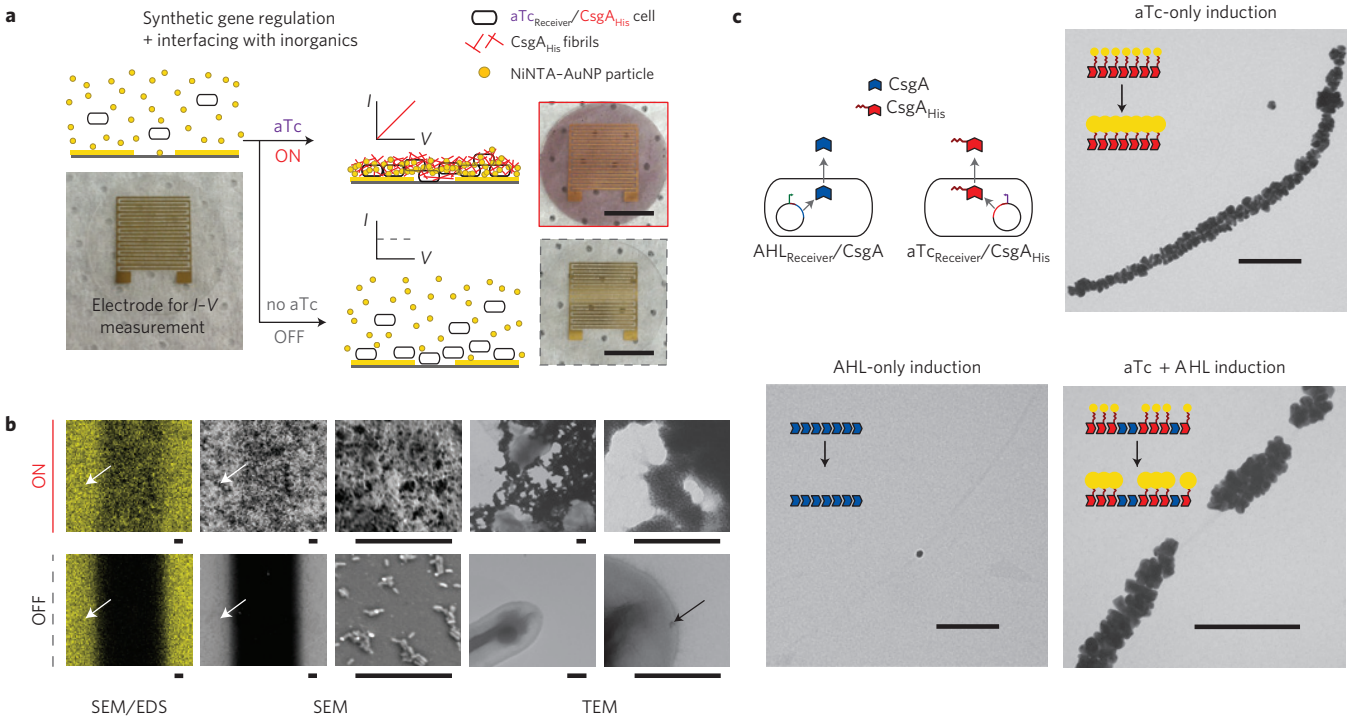

Figure 5 | Environmentally switchable conductive biofilms and cell-based synthesis of curli-templated nanowires and nanorods. **a**, We used aTc$_{Receiver}$/CsgA$_{His}$ cells to form amyloid fibrils composed of CsgA$_{His}$ in response to aTc. When combined with NiNTA-AuNPs, we created conductive biofilms that can be externally controlled as electrical switches. When aTc was added to aTc$_{Receiver}$/CsgA$_{His}$ cells grown in the presence of NiNTA-AuNPs, it triggered the formation of conductive biofilms on electrodes, with embedded 5nm gold particles giving biofilms a red colour ('ON', solid red box). However, in the absence of aTc, few cells adhered to the electrodes ('OFF', dashed grey box). Scale bars, 5 mm. **b**, SEM/EDS elemental mapping of the aTc-induced ON state for aTc$_{Receiver}$/CsgA$_{His}$ biofilms showed that networks of gold in the biofilms connected the electrodes (white arrows). SEM imaging showed that the biofilms bridged electrodes. TEM imaging showed networks of aggregated gold particles. In contrast, SEM/EDS mapping of the OFF state showed no gold networks, SEM imaging showed only scattered cells in the gap between electrodes, and TEM imaging showed only scattered and isolated gold particles (black arrow). Scale bars of scanning electron micrographs are 20 μm, and scale bars of transmission electron micrographs are 200 nm. **c**, A mixed population of aTc$_{Receiver}$/CsgA$_{His}$ and AHL$_{Receiver}$/CsgA cells produced curli templates for organizing either gold nanowires or gold nanorods when they were induced with aTc only or both aTc and AHL, respectively. NiNTA-AuNPs were patterned on CsgA$_{His}$ subunits within curli fibrils and then gold-enhanced. Scale bars, 200 nm.

We extended cell-based gold-particle patterning to create nanowires and nanorods via additional gold deposition. When aTc$_{Receiver}$/CsgA$_{His}$ and AHL$_{Receiver}$/CsgA cells were induced with only aTc, the resulting curli fibrils templated gold nanowires. When the cells were induced with both aTc and AHL, the resulting co-fibrils contained CsgA$_{His}$ and CsgA which templated consecutive gold nanorods (Fig. 5c). Gold nanorods have been studied for a range of applications because of their more broadly tunable absorption spectra compared to nanoparticles, which allows for peak absorption in the near-IR window used for *in vivo* imaging and photothermal ablation[27]. Moreover, via conjugation with targeting ligands and drug molecules, they can also act as targeted drug delivery vehicles for therapeutic and diagnostic applications[28,29].

We also used cellular biofabrication to create co-fibrils that assembled CdTe/CdS quantum dots (QDs) with gold nanoparticles, resulting in the modulation of QD fluorescence (Fig. 6). We leveraged interactions between the SpyCatcher protein and the SpyTag peptide tag[30], which results in the formation of covalent bonds, to dock QDs to fibrils displaying SpyTag. We used an orthogonal interaction between anti-FLAG antibodies and the FLAG affinity tag to dock 40 nm gold particles to fibrils displaying the FLAG tag. CsgA$_{SpyTag}$ fibrils were specifically bound by SpyCatcher-conjugated CdTe/CdS QDs (QD-SpyCatcher, Supplementary Fig. 21), while CsgA$_{FLAG}$ fibrils were specifically bound by anti-FLAG antibodies which were in turn bound by 40 nm gold particles conjugated with secondary antibodies (Fig. 6a and Supplementary Fig. 23a,b). AHL$_{Receiver}$/CsgA$_{SpyTag}$ and aTc$_{Receiver}$/CsgA$_{FLAG}$ strains were co-cultured in the presence of AHL, aTc, or both AHL and aTc. In the presence of AHL, fibrils produced by the cellular consortia bound only QD-SpyCatcher, whereas in the presence of aTc, the resulting fibrils bound only antibody-conjugated 40 nm gold particles (Fig. 6b and Supplementary Fig. 18). When both inducers were present, the fibrils co-assembled QDs with gold nanoparticles (Fig. 6b). Characterization with fluorescence-lifetime imaging microscopy (FLIM) revealed that co-assemblies of QDs and gold nanoparticles had altered fluorescence lifetimes and intensities compared to assemblies of QDs alone (Fig. 6c).

These results demonstrate that the behaviour of stimuli-responsive materials can be modulated by curli fibrils patterned with engineered cells. AuNP-QD heterostructures are of interest because plasmon–exciton interactions between plasmonic AuNPs and fluorescent QDs allow the tailoring of photon emission properties. By selecting appropriate materials and architectures, one can potentially tune emission intensity, directionality, and spectral profile for a range of applications[31–34].

In addition to organizing pre-formed nanomaterials, cell-fabricated curli fibrils can be used to grow inorganic materials. To demonstrate this, we engineered a strain that produced

© 2014 Macmillan Publishers Limited. All rights reserved.

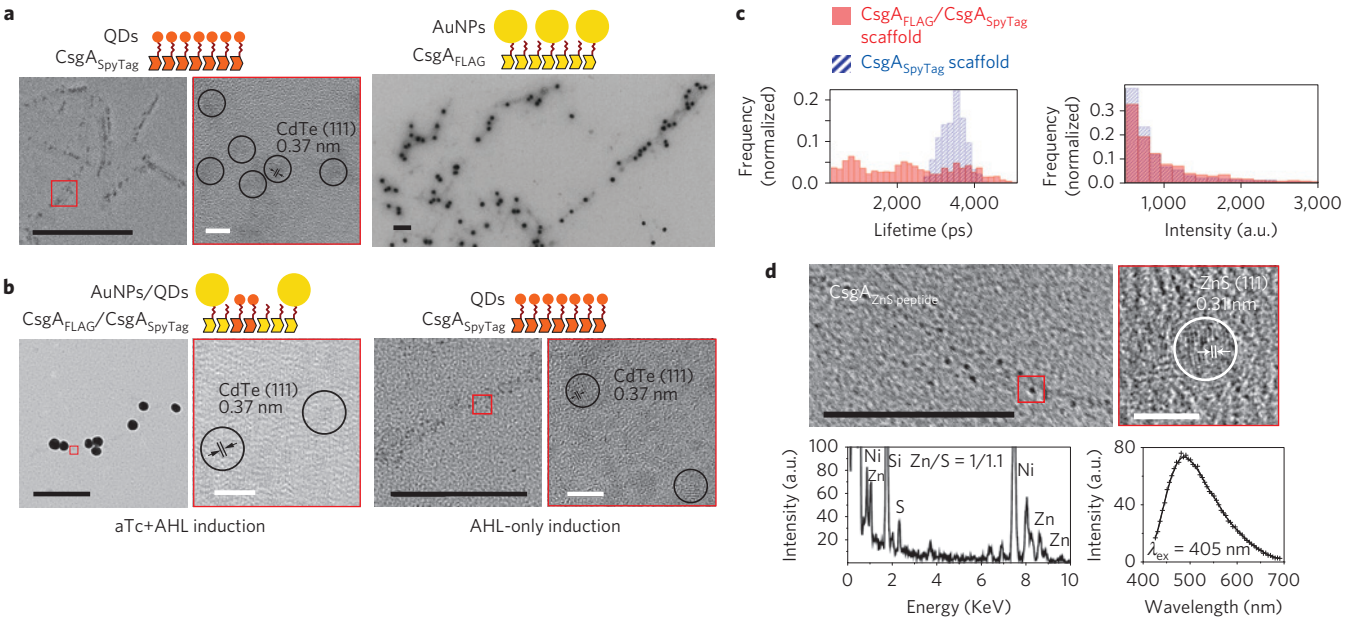

Figure 6 | Assembly and tuning of functional AuNP-QD heterostructures, and nucleation of fluorescent ZnS QDs on cell-synthesized curli fibrils. **a**, CsgA$_{SpyTag}$ fibrils specifically bind CdTe/CdS QDs conjugated to the SpyCatcher protein; the CdTe cores of QDs are seen under HRTEM. CsgA$_{FLAG}$ fibrils are specifically bound by anti-FLAG antibodies which are in turn bound by 40 nm AuNPs conjugated to secondary antibodies. CsgA fibrils do not bind either CdTe/CdS QDs conjugated to SpyCatcher or 40nm AuNPs conjugated to antibodies (Supplementary Fig. 23a,b). **b**, A mixed population of aTc$_{Receiver}$/CsgA$_{FLAG}$ and AHL$_{Receiver}$/CsgA$_{SpyTag}$ cells produced curli templates for either AuNP-QD heterostructures (co-fibrils of CsgA$_{FLAG}$ and CsgA$_{SpyTag}$) or QD-only assemblies (CsgA$_{SpyTag}$ fibrils), depending on whether they were induced by both aTc and AHL, or AHL only, respectively. **c**, Cell-patterned curli fibrils enable the tuning of stimuli-responsive biotic–abiotic materials. AuNP-QD assemblies patterned on CsgA$_{FLAG}$/CsgA$_{SpyTag}$ scaffolds (solid red bars) exhibited different fluorescence lifetime and intensity properties than QD-only assemblies patterned on CsgA$_{SpyTag}$ scaffolds (hashed blue bars). **d**, CsgA$_{ZnS\ peptide}$ fibrils nucleated ~5 nm nanoparticles with a cubic zinc blende ZnS (111) structure and approximately 1:1 ratio of zinc and sulphur. The particles were fluorescent, with an emission peak at 490 nm when excited at 405 nm. Control CsgA fibrils nucleated few such particles (Supplementary Fig. 23c). In **a**, **b** and **d** black scale bars, 200 nm, and white scale bars, 5 nm; the images outlined by red boxes are zoomed-in versions of the inset red boxes.

curli fibrils displaying a ZnS-nucleating peptide (CsgA$_{ZnS\ peptide}$; Supplementary Table 1; ref. 35). The resulting fibrils nucleated ~5 nm particles (Fig. 6d), whereas control fibrils composed of wild-type CsgA nucleated few such particles (Supplementary Fig. 23c). HRTEM images revealed that the nucleated particles had a cubic zinc blende ZnS (111) structure with a typical crystalline spacing of 0.31 nm (Fig. 6d). EDS analysis of elemental composition showed an approximately 1:1 ratio of zinc and sulphur (Fig. 6d). These data indicate that the particles are ZnS nanocrystals. The nanocrystals were fluorescent, with an emission peak at 490 nm when excited at 405 nm (Fig. 6d).

Outlook

We have shown that protein-based amyloid fibrils produced by living cells can be interfaced with different inorganic materials using a range of strategies. Beyond being a convenient model system with which to explore the applications of living systems to materials science, protein materials are of practical interest because they constitute a major class of biomaterials[36]. Protein materials can have programmable structures[37] and diverse functionalities, such as responsiveness to physicochemical stimuli[38], the ability to interact with living systems[39], and the ability to organize inorganic materials for expanded functionalities[35,40–42]. Amyloid fibrils can provide beneficial materials properties, such as resistance to degradation and mechanical strength comparable to that of steel[43]. As we have shown here, amyloid fibrils assembled by cells constitute a versatile scaffold that can co-organize and synthesize fluorescent QDs as well as gold nanowires, nanorods and nanoparticles. This approach could be generalized to include multiple CsgA variants with different functional properties and abilities to interact with various inorganic materials. In addition, curli fibrils with tunable structure and composition could be used as patterned scaffolds for multi-enzyme systems by displaying orthogonal affinity tags on curli fibrils which interact with different enzymes.

Most existing examples of protein biomaterials are assembled *in vitro* from chemically synthesized peptides or purified subunits and do not take full advantage of the fact that the materials' constituent subunits can be integrated into living cell communities. Living cells are natural platforms for engineering multiscale patterned materials because biology is organized in a hierarchical manner, from macromolecules (for example, proteins, nucleic acids, carbohydrates, lipids) to macromolecular assemblies (synthetic variants of which are used as nanomaterials[37,44–46]) to organelles, to cells, to tissues and, finally, to whole organisms. In fact, natural biological materials such as bone are hierarchically organized to fulfil varied functional requirements[1,9]. Thus, we have demonstrated an engineered cellular platform that synthesizes and patterns self-assembling materials with controllable functionality, structure and composition.

Using gene circuits within engineered biofilms for multiscale patterning of materials is a novel application area for synthetic biology. This work applies useful characteristics of multicellular communities to materials fabrication, and builds on previous efforts to engineer biofilms with synthetic circuits[10–16]. This strategy can be expanded to other cellular and biomaterials contexts for applications ranging from biointegrated electronic and optical devices[47–49] to tissue engineering scaffolds[50]. For example, cells

© 2014 Macmillan Publishers Limited. All rights reserved.

designed to compute and integrate complex signals could be used to assemble functional materials in response to their environment[18,19]. These 'smart' living materials could be composed of specialized cellular consortia that coordinate with each other for multi-functional materials synthesis. Mammalian cells capable of tunable, environmentally responsive synthesis of multiscale materials could be used to mimic the dynamic microenvironment of *in vivo* extracellular matrices[51] for tissue engineering. Our demonstration of a gradient material patterned at the nanoscale and the millimetre scale could be used to biofabricate functionally graded materials[52]. Moreover, leveraging hierarchical organization from biology for multiscale patterning should complement other strategies for materials synthesis that require directed intervention[53], such as 3D printing[52]. Repeated materials-synthesis processes or environmentally switchable behaviours could be achieved by triggering biofilm disassembly[12,13,54].

In summary, by integrating synthetic gene networks in engineered cells with extracellular protein biomaterials, living materials with environmental responsiveness, tunable functionalities, multiscale patterning, and even the ability to self-heal and remodel could be realized. In such materials, there would be a division of labour between cells (providing functionalities of living systems)[55], extracellular protein materials (providing spatial patterning and structural integrity), and interfaced inorganic materials (providing functionalities of non-living systems). Thus, we expect that engineering artificial cellular consortia, such as biofilms, to synthesize and organize heterogeneous functional materials, will enable the realization of smart composite materials that combine the properties of living and non-living systems.

Methods

Culture conditions. Seed cultures were inoculated from glycerol stocks and grown in LB-Miller medium for 12 h at 37 °C. Experimental cultures were grown at 30 °C in M63 minimal medium supplemented with 1mM $MgSO_4$ and with 0.2% w/v glucose or 0.2% w/v glycerol. For inducing conditions, anhydrotetracycline (Sigma) at concentrations of 1–250 ng ml^{-1} and *N*-(β-ketocaproyl)-L-homoserine lactone (Sigma) at concentrations of 1–1,000 nM were used.

Anti-CsgA immuno-labelling. Rabbit anti-CsgA primary antibody (M. Chapman, University of Michigan) was used at 1:1,000 dilution, goat anti-rabbit secondary antibody conjugated to 10 nm gold particles (Sigma) was used at 1:10 dilution.

NiNTA-AuNP labelling. For specific binding of NiNTA-AuNP (Nanoprobes) to histidine tags displayed on curli fibrils, buffer consisting of 1X PBS with 0.487 M NaCl, 80 mM imidazole, and 0.2v/v% Tween20 was used.

Conductive biofilm conductance measurement. Interdigitated electrodes (IDEs) for measuring biofilm conductance were created by sputtering gold through custom shadowing masks (Tech-Etch) onto Thermanox coverslips (Nunc). IDEs were placed in 24-well plate wells and conductive biofilms grown by adding 100 nM NiNTA-AuNP into culture medium. After biofilm culture, IDEs were washed by repeatedly immersing in double distilled H_2O, laid on a flat surface, and allowed to air dry for three days. A Keithley 4200 picoammeter with a two-point probe was used to carry out a voltage sweep.

Gold nanowire and nanorod synthesis. Gold was specifically deposited on NiNTA-AuNP chains using GoldEnhance EM kit (Nanoprobes).

Specific binding of QD-SpyCatcher. For specific binding of CdTe/CdS-SpyCatcher to SpyTag peptide tags displayed on curli fibrils, buffer consisting of 1X PBS + 350 mM NaCl + 0.3v/v% Tween20 was used.

Specific binding of antibody-conjugated 40 nm AuNP. Rabbit anti-FLAG primary antibody (Sigma) was used at 1:250 dilution, goat anti-rabbit secondary antibody conjugated to 40 nm AuNPs (Abcam) was used at 1:10 dilution.

Zinc sulphide nanocrystal synthesis. Fibril samples were incubated with 1 μM $ZnCl_2$ at RT for 12 h, followed by addition of 1 μM Na_2S. Samples were then incubated at 0 °C for 24 h by packing in ice and placing in a 4 °C room, and subsequently allowed to age for 12 h at room temperature.

TEM. Samples were deposited on 200-mesh formvar/carbon coated nickel TEM grids and stained with 2% uranyl acetate. TEM images were obtained on an FEI Tecnai Spirit transmission electron microscope operated at 80 kV accelerating voltage. High-resolution transmission electron microscopy (HRTEM) and energy-dispersive X-ray spectroscopy (EDS) were performed on a JEOL 2010F electron microscope operating at 200 kV.

SEM. Samples were imaged with a JEOL JSM-6010LA scanning electron microscope operated at 10 kV accelerating voltage. Images were obtained in secondary electron imaging (SEI) mode, and elemental mapping was performed with energy-dispersive X-ray spectroscopy (EDS).

Fluorescence microscopy. Fluorescence-lifetime imaging microscopy (FLIM) was performed with a Zeiss 710 NLO multiphoton microscope with a ×20 objective and connected to a time-correlated single-photon counting system (Becker and Hickl). The excitation source was a two-photon laser (Coherent Chameleon Vision II) tuned to 800 nm, and emission was detected through a 590–650 nm bandpass filter. Lambda scan analysis of fluorescent ZnS nanocrystals was performed with a Zeiss LSM 710 NLO Laser Scanning Confocal with a ×10 objective and a 405 nm excitation laser.

Received 20 June 2013; accepted 11 February 2014; published online 23 March 2014

References

1. Fratzl, P. & Weinkamer, R. Nature's hierarchical materials. *Prog. Mater. Sci.* **52,** 1263–1334 (2007).
2. Kollmannsberger, P., Bidan, C. M., Dunlop, J. W. C. & Fratzl, P. The physics of tissue patterning and extracellular matrix organisation: How cells join forces. *Soft Matter* **7,** 9549–9560 (2011).
3. Stevens, M. M. & George, J. H. Exploring and engineering the cell surface interface. *Science* **310,** 1135–1138 (2005).
4. O'Toole, G., Kaplan, H. B. & Kolter, R. Biofilm formation as microbial development. *Annu. Rev. Microbiol.* **54,** 49–79 (2000).
5. Epstein, A. K., Pokroy, B., Seminara, A. & Aizenberg, J. Bacterial biofilm shows persistent resistance to liquid wetting and gas penetration. *Proc. Natl Acad. Sci. USA* **108,** 995–1000 (2011).
6. Belcher, A. M. *et al.* Control of crystal phase switching and orientation by soluble mollusc-shell proteins. *Nature* **381,** 56–58 (1996).
7. Su, X. W., Zhang, D. M. & Heuer, A. H. Tissue regeneration in the shell of the Giant Queen Conch, *Strombus gigas*. *Chem. Mater.* **16,** 581–593 (2004).
8. Aizenberg, J. *et al.* Skeleton of *Euplectella* sp: structural hierarchy from the nanoscale to the macroscale. *Science* **309,** 275–278 (2005).
9. Weiner, S. & Wagner, H. D. The material bone: Structure mechanical function relations. *Annu. Rev. Mater. Sci.* **28,** 271–298 (1998).
10. Brenner, K. & Arnold, F. H. Self-organization, layered structure, and aggregation enhance persistence of a synthetic biofilm consortium. *PloS ONE* **6,** e16791 (2011).
11. Brenner, K., Karig, D. K., Weiss, R. & Arnold, F. H. Engineered bidirectional communication mediates a consensus in a microbial biofilm consortium. *Proc. Natl Acad. Sci. USA* **104,** 17300–17304 (2007).
12. Hong, S. H. *et al.* Synthetic quorum-sensing circuit to control consortial biofilm formation and dispersal in a microfluidic device. *Nature Commun.* **3,** 613 (2012).
13. Ma, Q., Yang, Z., Pu, M., Peti, W. & Wood, T. K. Engineering a novel c-di-GMP-binding protein for biofilm dispersal. *Environ. Microbiol.* **13,** 631–642 (2011).
14. Lee, J., Jayaraman, A. & Wood, T. K. Indole is an inter-species biofilm signal mediated by SdiA. *BMC Microbiol.* **7,** 42 (2007).
15. Payne, S. *et al.* Temporal control of self-organized pattern formation without morphogen gradients in bacteria. *Mol. Syst. Biol.* **9,** 697 (2013).
16. Payne, S. & You, L. Engineered cell–cell communication and its applications. *Adv. Biochem. Eng./Biotechnol.* http://dx.doi.org/10.1007/10_2013_249 (2013).
17. Barnhart, M. M. & Chapman, M. R. Curli biogenesis and function. *Annu. Rev. Microbiol.* **60,** 131–147 (2006).
18. Callura, J. M., Cantor, C. R. & Collins, J. J. Genetic switchboard for synthetic biology applications. *Proc. Natl Acad. Sci. USA* **109,** 5850–5855 (2012).
19. Prigent-Combaret, C. *et al.* Developmental pathway for biofilm formation in curli-producing *Escherichia coli* strains: Role of flagella, curli and colanic acid. *Environ. Microbiol.* **2,** 450–464 (2000).
20. Vidal, O. *et al.* Isolation of an *Escherichia coli* K-12 mutant strain able to form biofilms on inert surfaces: Involvement of a new *ompR* allele that increases curli expression. *J. Bacteriology* **180,** 2442–2449 (1998).
21. Hung, C. *et al. Escherichia coli* biofilms have an organized and complex extracellular matrix structure. *mBio* **4,** e00645–e00613 (2013).

© 2014 Macmillan Publishers Limited. All rights reserved.

22. Wang, X., Hammer, N. D. & Chapman, M. R. The molecular basis of functional bacterial amyloid polymerization and nucleation. *J. Biol. Chem.* **283,** 21530–21539 (2008).
23. Basu, S., Gerchman, Y., Collins, C. H., Arnold, F. H. & Weiss, R. A synthetic multicellular system for programmed pattern formation. *Nature* **434,** 1130–1134 (2005).
24. Bacchus, W *et al.* Synthetic two-way communication between mammalian cells. *Nature Biotechnol.* **30,** 991–996 (2012).
25. Tabor, J. J. *et al.* A synthetic genetic edge detection program. *Cell* **137,** 1272–1281 (2009).
26. Liu, C. *et al.* Sequential establishment of stripe patterns in an expanding cell population. *Science* **334,** 238–241 (2011).
27. Jang, B., Park, J. Y., Tung, C. H., Kim, I. H. & Choi, Y. Gold nanorod-photosensitizer complex for near-infrared fluorescence imaging and photodynamic/photothermal therapy *in vivo*. *ACS Nano* **5,** 1086–1094 (2011).
28. Dreaden, E. C. *et al.* Small molecule-gold nanorod conjugates selectively target and induce macrophage cytotoxicity towards breast cancer cells. *Small* **8,** 2819–2822 (2012).
29. Libutti, S. K. *et al.* Phase I and pharmacokinetic studies of CYT-6091, a novel PEGylated colloidal gold-rhTNF nanomedicine. *Clinical Cancer Research: An Official J. Am. Assoc. Can. Res.* **16,** 6139–6149 (2010).
30. Zakeri, B. *et al.* Peptide tag forming a rapid covalent bond to a protein, through engineering a bacterial adhesin. *Proc. Natl Acad. Sci. USA* **109,** E690–E697 (2012).
31. Polman, A. & Atwater, H. A. Photonic design principles for ultrahigh-efficiency photovoltaics. *Nature Mater.* **11,** 174–177 (2012).
32. Reineck, P. *et al.* A solid-state plasmonic solar cell via metal nanoparticle self-assembly. *Adv. Mater.* **24,** 4750–4755 (2012).
33. Curto, A. G. *et al.* Unidirectional emission of a quantum dot coupled to a nanoantenna. *Science* **329,** 930–933 (2010).
34. Yuan, Z. L. *et al.* Electrically driven single-photon source. *Science* **295,** 102–105 (2002).
35. Mao, C. *et al.* Viral assembly of oriented quantum dot nanowires. *Proc. Natl Acad. Sci. USA* **100,** 6946–6951 (2003).
36. Zhang, S. G. Fabrication of novel biomaterials through molecular self-assembly. *Nature Biotechnol.* **21,** 1171–1178 (2003).
37. King, N. P. *et al.* Computational design of self-assembling protein nanomaterials with atomic level accuracy. *Science* **336,** 1171–1174 (2012).
38. Mart, R. J., Osborne, R. D., Stevens, M. M. & Ulijn, R. V. Peptide-based stimuli-responsive biomaterials. *Soft Matter* **2,** 822–835 (2006).
39. Webber, M. J. *et al.* Supramolecular nanostructures that mimic VEGF as a strategy for ischemic tissue repair. *Proc. Natl Acad. Sci. USA* **108,** 13438–13443 (2011).
40. So, C. R., Tamerler, C. & Sarikaya, M. Adsorption, diffusion, and self-assembly of an engineered gold-binding peptide on Au(111) investigated by atomic force microscopy. *Angew. Chem. Int. Ed.* **48,** 5174–5177 (2009).
41. Channon, K. J., Devlin, G. L. & MacPhee, C. E. Efficient energy transfer within self-assembling peptide fibers: A route to light-harvesting nanomaterials. *J. Am. Chem. Soc.* **131,** 12520–12521 (2009).
42. Scheibel, T. *et al.* Conducting nanowires built by controlled self-assembly of amyloid fibers and selective metal deposition. *Proc. Natl Acad. Sci. USA* **100,** 4527–4532 (2003).
43. Smith, J. F., Knowles, T. P., Dobson, C. M., Macphee, C. E. & Welland, M. E. Characterization of the nanoscale properties of individual amyloid fibrils. *Proc. Natl Acad. Sci. USA* **103,** 15806–15811 (2006).
44. Felgner, P. L. *et al.* Lipofection: A highly efficient, lipid-mediated DNA-transfection procedure. *Proc. Natl Acad. Sci. USA* **84,** 7413–7417 (1987).
45. Winfree, E., Liu, , F., Wenzler, L. A. & Seeman, N. C. Design and self-assembly of two-dimensional DNA crystals. *Nature* **394,** 539–544 (1998).
46. Rothemund, P. W. Folding DNA to create nanoscale shapes and patterns. *Nature* **440,** 297–302 (2006).
47. Tian, B. *et al.* Macroporous nanowire nanoelectronic scaffolds for synthetic tissues. *Nature Mater.* **11,** 986–994 (2012).
48. Hwang, S. W. *et al.* A physically transient form of silicon electronics. *Science* **337,** 1640–1644 (2012).
49. Amsden, J. J. *et al.* Rapid nanoimprinting of silk fibroin films for biophotonic applications. *Adv. Mater.* **22,** 1746–1749 (2010).
50. Lutolf, M. P. & Hubbell, J. A. Synthetic biomaterials as instructive extracellular microenvironments for morphogenesis in tissue engineering. *Nature Biotechnol.* **23,** 47–55 (2005).
51. Prewitz, M. C. *et al.* Tightly anchored tissue-mimetic matrices as instructive stem cell microenvironments. *Nature Methods* **10,** 788–794 (2013).
52. Chiu, W. K. & Yu, K. M. Direct digital manufacturing of three-dimensional functionally graded material objects. *Computer-Aided Design* **40,** 1080–1093 (2008).
53. Xia, Y., Rogers, J. A., Paul, K. E. & Whitesides, G. M. Unconventional methods for fabricating and patterning nanostructures. *Chem. Rev.* **99,** 1823–1848 (1999).
54. Kolodkin-Gal, I. *et al.* D-amino acids trigger biofilm disassembly. *Science* **328,** 627–629 (2010).
55. Gubeli, R. J., Burger, K. & Weber, W. Synthetic biology for mammalian cell technology and materials sciences. *Biotechnol. Adv.* **31,** 68–78 (2013).

Acknowledgements

We thank J. J. Collins (Biomedical Engineering, Boston University) for donating riboregulator plasmids, R. Weiss (Electrical Engineering and Computer Science, MIT) for the gift of a LuxI plasmid, C. Dorel (Biosciences Department, INSA Lyon) for the gift of *E. coli* MG1655 *ompR234*, M. Chapman (Department of Molecular, Cellular, and Developmental Biology, University of Michigan Ann Arbor) for the gift of anti-CsgA antibodies, K. Ribbeck (Department of Biological Engineering, MIT) for use of confocal microscopy facilities, and L. Cameron (Confocal and Light Microscopy Core, Dana Farber Cancer Institute) for assistance with FLIM. We thank C. Zhong, K. Lowenhaupt and P. Siuti from the Lu lab, S. Keating from the lab of N. Oxman (Media Lab, MIT), K. Frederick from the lab of S. Lindquist, S. Lindquist (Whitehead Institute), and E. Dreaden from the lab of P. Hammond (Chemical Engineering, MIT) for helpful discussions. We thank C. Zhong from the Lu lab for the gift of purified CsgA protein. We also thank M. Mimee and O. Purcell from the Lu lab for a close reading of this manuscript. This work was supported by the Office of Naval Research and the Army Research Office. This work was also supported in part by the MRSEC Program of the National Science Foundation under award number DMR-0819762. A.Y.C. acknowledges graduate research support from the Hertz Foundation, the Department of Defense, and NIH Medical Scientist Training Program grant T32GM007753. A.N.B. acknowledges support from NIH-NIEHS Training Grant in Toxicology 5 T32 ES7020-37. T.K.L. acknowledges support from the Presidential Early Career Award for Scientists and Engineers and the NIH New Innovator Award (1DP2OD008435).

Author contributions

T.K.L. and A.Y.C. conceived the experiments. A.Y.C., Z.D., A.N.B., U.O.S.S., M.Y.L. and R.J.C. performed the experiments, A.Y.C., Z.D., A.N.B. and T.K.L. analysed the data, discussed results, and wrote the manuscript.

Additional information

Supplementary information is available in the online version of the paper. Reprints and permissions information is available online at www.nature.com/reprints. Correspondence and requests for materials should be addressed to T.K.L.

Competing financial interests

T.K.L. and A.Y.C. have filed a provisional application based on this work with the US Patent and Trademark Office.

© 2014 Macmillan Publishers Limited. All rights reserved.